An Effective Fully Polarizable QM/MM Approach to Model Vibrational Circular Dichroism Spectra of Systems in Aqueous Solution

Tommaso Giovannini,[†] Marta Olszòwka,[‡] and Chiara Cappelli[*,†]

Scuola Normale Superiore, Piazza dei Cavalieri 7, 56126 Pisa, Italy, and Dipartimento di Chimica e Chimica Industriale, Università di Pisa, Via Moruzzi 3, 56124 Pisa, Italy.

E-mail: chiara.cappelli@sns.it

Abstract

We propose a methodology, based on the combination of classical Molecular Dynamics (MD) simulations with a fully polarizable Quantum Mechanical (QM)/Molecular Mechanics (MM)/Polarizable Continuum Model (PCM) Hamiltonian to calculate Vibrational Circular Dichroism (VCD) spectra of chiral systems in aqueous solution. Polarization effects are included in the MM force field by exploiting an approach based on Fluctuating Charges (FQ). By performing the MD, the description of the solvating environment is enriched by taking into account the dynamical aspects of the solute-solvent interactions. On the other hand, the QM/FQ/PCM calculation of the VCD spectrum ensures an accurate description of the electronic density of the solute and a proper account for the specific interactions in solution. The application of our approach to (R)-methyloxirane and (L)-alanine in aqueous solution gives calculated spectra in

[*]To whom correspondence should be addressed

[†]Scuola Normale Superiore, Piazza dei Cavalieri 7, 56126 Pisa, Italy

[‡]Dipartimento di Chimica e Chimica Industriale, Università di Pisa, Via Moruzzi 3, 56124 Pisa, Italy.

remarkable agreement with their experimental counterparts and a substantial improvement with respect to the same spectra calculated with the PCM.

1 Introduction

The measurement of the chiroptical spectroscopic signals has become a common practice both in the academia and in industry to assign the molecular absolute configuration.[1] Such signals arise from the response of the system to polarized light, which is of opposite sign for the two enantiomers. Different families of responses exist, such as the Optical Rotation (OR) and other chiroptical spectroscopies, which are based on the different absorption/emission/scattering of the right and left components of the circularly polarized light. In case of absorption, within the range of electronic transitions (UV-VIS) this spectroscopy is named Electronic Circular Dichroism (ECD), whereas in the infrared (IR) range it is named Vibrational Circular Dichroism (VCD). The latter, together with the Raman Optical Activity (ROA), have obtained a positive outcome in terms of reliability and applicability, as it is represented by the number of recent works reporting this subject.[2–12]

The use of VCD to assign the absolute configuration is always accompanied by computations: quantum mechanical (QM) approaches play in this field a relevant role.[13] In fact, the required feature of any computational method is the reliability and the accuracy in the prediction of experimental data. In order to obtain a quantitative and qualitative description of the chiroptical response, a QM description of the target molecule is needed, and the account of electronic correlation has been reported to be substantial.[14] A good compromise between accuracy and computational cost can be achieved by DFT (Density Functional Theory) exploiting hybrid functionals, which can reproduce well response properties as the ones here considered.[15–20]

Chiroptical properties, and especially VCD, are rarely measured on a sample in the gas phase, while the measurement in condensed phase is more common. The role of solvation is crucial in the response of a molecular system to an external radiation, as it is shown by several examples taken from the common experience: solvatochromism is, for instance, a very common feature of most chromophores; chiral molecules can change their rotatory strength, even to the point that they change from dextrorotatory in the gas phase to levorotatory in

solution or vice-versa.[16,19,21,22]

For these reasons, several methods to include the effects of the external environment in QM calculations have been developed. In this context, focused models based on a multiscale approach have covered an important role.[23–25] The standard procedure, which nowadays constitutes the state-of-the-art of most studies, is to resort to a continuous description of the solvent, such as that yielded by the Polarizable Continuum Model (PCM). Such an approach has the advantage of low computational costs, however it gives a reasonably good description for solute-solvent interactions for systems dominated by electrostatic effects.[16,26–28] On the contrary, in case of strongly interacting solute-solvent couples, such as those dominated by hydrogen-bonding interactions, PCM is generally unable to correctly reproduce experimental data.[16,29] This is obviously a strong limitation of continuum models applied to chiral systems, because the natural environment of numerous systems is the aqueous solution (proteins, nucleic acids, drugs, etc.).

In order to improve the continuous description, an explicit treatment of the solvent is needed and this is generally solved by resorting to QM/Molecular Mechanics (MM) methods, where the atomistic description of the solvent is recovered.[30–36] In standard MM force fields, all the atoms are treated as fixed point charges. A better description is obtained by introducing the possibility for the atoms to be polarized by an external (also local) field (polarizable force field). Several polarizable force fields have been developed,[37] and in this work, we will focus on the three layer polarizable QM/MM/PCM model, named QM/FQ/PCM, which uses the force field proposed by Rick *et al.*[38–40] where the MM portion is described as Fluctuating point charges (FQ) that can vary in agreement with the *Electronegativity Equalization Principle* (EEP). This was first proposed by Sanderson and it states that, at equilibrium, the instantaneous electronegativity of each atom has the same value.[41]

The QM/FQ/PCM approach has recently been extended to the calculation of various molecular properties,[29,42–45] thanks to the implementation of a fully variational treatment, of analytical first and second derivatives, and magnetic response properties with GIAOs.[45] The

QM/FQ/PCM has already been shown to accurately model some of the systems where PCM and other continuum models completely fail.[17,46–50] In this paper, its further extension to VCD spectra is reported for the first time.

The paper is organized in the following way. In the next section the theoretical and computational fundamentals of the QM/FQ/PCM model are recalled, and its extension to calculate VCD rotational strengths is reported. Then, the potentialities of the method are shown for the particular cases of (R)-methyloxirane and (L)-alanine in aqueous solution. For such systems, the comparison with computational data obtained by exploiting continuum solvation methodologies and experimental spectra is reported. Some conclusions and future perspectives close the manuscript.

2 Theory

2.1 The QM/FQ/PCM approach

The FQ approach[29,42] is particularly suitable to be employed within a QM/MM framework because of its connection both with quantum mechanics and classical electrostatics. The model is based on the concepts of atomic hardness and electronegativity, which can be rigorously defined within the DFT,[51,52] and the electronic distribution is represented in terms of a set of classical atomic charges depending on the electrostatic potential.[38,39]

The FQ approach represents the polarization of a classical, atomic system by endowing each atom with a fluctuating charge, of which the value depends on the environment[38–40] according to the electronegativity equalization principle[51,53] which states that, at equilibrium, the instantaneous electronegativity χ of each atom have the same value.[41,51] The FQs (q) can

be defined as those minimizing the following functional[42]

$$F(\mathbf{q},\lambda) = \sum_{\alpha,i} q_{\alpha i}\chi_{\alpha i} + \frac{1}{2}\sum_{\alpha,i}\sum_{\beta,j} q_{\alpha i}J_{\alpha i,\beta j}q_{\beta j} + \sum_{\alpha}\lambda_{\alpha}(\sum_{i} q_{\alpha i} - Q_{\alpha})$$
$$= \mathbf{q}^{\dagger}\boldsymbol{\chi} + \frac{1}{2}\mathbf{q}^{\dagger}\mathbf{J}\mathbf{q} + \boldsymbol{\lambda}^{\dagger}\mathbf{q} \quad (1)$$

where the Greek indices α run over molecules and the Latin ones i over the atoms of each molecule. $\boldsymbol{\lambda}$ is a set of Lagrangian multipliers used to impose charge conservation constraints. $\mathbf{J}$ is the charge interaction kernel. There are several ways to treat this term[52–55] and in our implementation the Ohno kernel[56] is exploited, however, the implementation is general enough to allow other kernels to be exploited:

$$J_{ij}(r_{ij}) = \frac{\eta_{ij}}{[1+\eta_{ij}^2 r_{ij}^2]^{1/2}} \quad (2)$$

η_i is the hardness of the i-th atom and

$$\eta_{ij} = \frac{\eta_i + \eta_j}{2}$$

is the average of the atomic hardnesses of atoms i and j and $r_{ij} = |\mathbf{r}_i - \mathbf{r}_j|$ is the distance between two MM atoms.

The stationarity conditions of the functional in eq.1 are defined through the following equation[42]

$$\mathbf{D}\mathbf{q}_{\boldsymbol{\lambda}} = -\mathbf{C}_Q \quad (3)$$

where $\mathbf{C}_Q$ collects atomic electronegativities and total charge constraints, whereas charges and Lagrange multipliers are collected in $\mathbf{q}_{\boldsymbol{\lambda}}$ and $\mathbf{D}$ includes the $\mathbf{J}$ matrix and the Lagrangian blocks.

By following the general philosophy of the so-called "focused" models, in the QM/FQ/PCM

model, a classical interaction between the FQs and the QM density is considered:[43]

$$E_{\mathrm{QM/MM}} = \sum_{i=1}^{N_q} V_{\mathrm{QM}}[\rho](\mathbf{r}_i) q_i \tag{4}$$

where $V_{\mathrm{QM}}[\rho](\mathbf{r}_i)$ is the electrostatic potential due to the QM density of charge at the i-th FQ q_i placed at $\mathbf{r}_i$.

If a self-consisten-field (SCF) description of the QM portion is adopted, the global QM/MM energy functional reads:[43,44,57]

$$\mathcal{E}[\mathbf{P},\mathbf{q},\boldsymbol{\lambda}] = \mathrm{tr}\mathbf{h}\mathbf{P} + \frac{1}{2}\mathrm{tr}\mathbf{P}\mathbf{G}(\mathbf{P}) + \mathbf{q}^\dagger\boldsymbol{\chi} + \frac{1}{2}\mathbf{q}^\dagger\mathbf{J}\mathbf{q} + \boldsymbol{\lambda}^\dagger\mathbf{q} + \mathbf{q}^\dagger\mathbf{V}(\mathbf{P}) \tag{5}$$

where $\mathbf{h}$ and $\mathbf{G}$ are the usual one- and two-electron integral matrices, and $\mathbf{P}$ is the QM density matrix.

The FQs consistent with the QM density are obtained by solving the following equation

$$\mathbf{D}\mathbf{q}_{\boldsymbol{\lambda}} = -\mathbf{C}_Q - \mathbf{V}_{\mathrm{FQ}}(\mathbf{P}) \tag{6}$$

which includes the coupling term $\mathbf{V}_{\mathrm{FQ}}(\mathbf{P})$ between the QM and MM moieties.

A third layer may be included in the model, by employing a continuum description of the outer solvent shell,[21] which also allows for an effective and physically suitable way to enforce nonperiodic boundary conditions (nPBC).[42] By resorting to the variational formalism of the PCM,[58,59] the functional to be minimized reads

$$\begin{aligned}\mathcal{E}[\mathbf{P},\mathbf{q},\boldsymbol{\lambda},\boldsymbol{\sigma}] &= \mathrm{tr}\mathbf{h}\mathbf{P} + \frac{1}{2}\mathrm{tr}\mathbf{P}\mathbf{G}(\mathbf{P}) + \mathbf{q}^\dagger\boldsymbol{\chi} + \frac{1}{2}\mathbf{q}^\dagger\mathbf{J}\mathbf{q} + \boldsymbol{\lambda}^\dagger\mathbf{q} + \mathbf{q}^\dagger\mathbf{V}_{\mathrm{FQ}}(\mathbf{P}) \\ &+ \frac{1}{2f(\varepsilon)}\boldsymbol{\sigma}^\dagger\mathbf{S}\boldsymbol{\sigma} + \boldsymbol{\sigma}^\dagger\mathbf{V}_{\mathrm{PCM}}(\mathbf{P}) + \boldsymbol{\sigma}^\dagger\boldsymbol{\Omega}\mathbf{q}\end{aligned} \tag{7}$$

where $\mathbf{V}_{\mathrm{FQ}}$ and $\mathbf{V}_{\mathrm{PCM}}$ denote the QM solute's potential calculated at the FQs and at the PCM discretization points, while $\mathbf{S}$ and $\boldsymbol{\Omega}$ represent the Coulomb interaction of the PCM

charges ($\boldsymbol{\sigma}$) with themselves and with the FQs, respectively. $\frac{1}{2f(\varepsilon)} = \frac{\varepsilon-1}{\varepsilon}$ is a scaling factor depending on the continuum dielectric properties. Similarly to Eq.6, the FQs and the PCM charges are simultaneously obtained by solving the following equations:

$$\begin{pmatrix} \mathbf{D} & \boldsymbol{\Omega}^{\dagger} \\ \boldsymbol{\Omega} & \mathbf{S}/f(\varepsilon) \end{pmatrix} \begin{pmatrix} \mathbf{q}_{\boldsymbol{\lambda}} \\ \boldsymbol{\sigma} \end{pmatrix} = - \begin{pmatrix} \mathbf{C} \\ \mathbf{0} \end{pmatrix} - \begin{pmatrix} \mathbf{V}_{\mathrm{FQ}}(\mathbf{P}) \\ \mathbf{V}_{\mathrm{PCM}}(\mathbf{P}) \end{pmatrix} \tag{8}$$

Once the basic QM/FQ/PCM approach is set up, the extension to spectroscopic and transition properties is obtained through the definition of analytical energy derivatives and response equations to electric and magnetic perturbations. Because we aim at calculating the properties of a given molecular system interacting with an external solvating environment, we can resort to the physical framework of the so-called "focused models", which in this case implies that the external perturbation (i.e., the electric/magnetic field or a nuclear displacement) only acts on the QM portion of the system, whereas the environment is only indirectly affected. Therefore, only indirect effects on the MM part through the perturbation on the QM density are considered.

The QM/MM energy first derivative with respect to a perturbation x (i.e. a nuclear displacement) acting on the QM portion can be expressed as[44,60]

$$\mathcal{E}^{x}(\mathbf{P},\mathbf{q},\lambda) = \mathrm{tr}\ \mathbf{h}^{x}\mathbf{P} + \frac{1}{2}\mathrm{tr}\ \mathbf{G}^{(x)}(\mathbf{P})\mathbf{P} + \mathbf{q}^{\dagger}\mathbf{V}^{(x)}_{FQ}(\mathbf{P}) + \boldsymbol{\sigma}^{\dagger}\mathbf{V}^{(x)}_{PCM}(\mathbf{P}) - \mathrm{tr}\mathbf{W}\mathbf{S}^{x}_{oo} \tag{9}$$

which requires, with respect to the standard calculation *in vacuo*, the computation of additional terms depending on FQ and PCM charges.

The energy second derivative with respect to perturbations x, y, once again acting on the

QM part of the system, can be obtained by further differentiating the above equation[44]

$$\begin{aligned}\mathcal{E}^{xy} &= \left[\mathbf{h}^{xy} + \frac{1}{2}\mathbf{G}^{(xy)}(\mathbf{P}) + \mathbf{q}^{\dagger}\mathbf{V}_{FQ}^{xy} + \boldsymbol{\sigma}^{\dagger}\mathbf{V}_{PCM}^{xy}\right]\mathbf{P} - \text{tr }\mathbf{W}\mathbf{S}^{xy} - \text{tr }\mathbf{W}^{y}\mathbf{S}^{x} \\ &+ \left[\mathbf{h}^{x} + \mathbf{G}^{(x)}(\mathbf{P}) + \mathbf{q}^{\dagger}\mathbf{V}_{FQ}^{x} + \boldsymbol{\sigma}^{\dagger}\mathbf{V}_{PCM}^{x}\right]\mathbf{P}^{y} \\ &+ \mathbf{q}^{y\dagger}\mathbf{V}_{FQ}^{x}\mathbf{P} + \boldsymbol{\sigma}^{y\dagger}\mathbf{V}_{PCM}^{x}\mathbf{P} \end{aligned} \tag{10}$$

which requires the computation of the perturbed density matrix, which is accessible through a Coupled Perturbed Hartree-Fock or Kohn-Sham (CPHF/KS) procedure by solving a modified set of equations including FQ/PCM terms.[43,44] In the construction of the CPHF equations the Fock matrix derivative is used:

$$\begin{aligned}\tilde{\mathbf{F}}^{x} &= \mathbf{h}^{x} + \mathbf{G}^{(x)}(\mathbf{P}) + \mathbf{q}^{\dagger}\mathbf{V}_{FQ}^{x} + \boldsymbol{\sigma}^{\dagger}\mathbf{V}_{PCM}^{x} + \mathbf{G}(\mathbf{P}^{x}) + \mathbf{V}_{FQ}^{\dagger}\mathbf{q}^{x} + \mathbf{V}_{PCM}^{\dagger}\boldsymbol{\sigma}^{x} \\ &= \mathbf{F}^{(x)} + \mathbf{q}^{\dagger}\mathbf{V}_{FQ}^{x} + \boldsymbol{\sigma}^{\dagger}\mathbf{V}_{PCM}^{x} + \mathbf{G}(\mathbf{P}^{x}) + \mathbf{V}_{FQ}^{\dagger}\mathbf{q}^{x} + \mathbf{V}_{PCM}^{\dagger}\boldsymbol{\sigma}^{x} \end{aligned} \tag{11}$$

which is included in the $\tilde{\mathbf{Q}}_X$ and $\tilde{\mathbf{Q}}_Y$ terms of the following equation:

$$\begin{pmatrix} \tilde{\mathbf{A}} & \tilde{\mathbf{B}} \\ \tilde{\mathbf{B}}^{*} & \tilde{\mathbf{A}}^{*} \end{pmatrix} \begin{pmatrix} \mathbf{X} \\ \mathbf{Y} \end{pmatrix} = \begin{pmatrix} \tilde{\mathbf{Q}}_X \\ \tilde{\mathbf{Q}}_Y \end{pmatrix} \tag{12}$$

The solution of this set of equations yields the density matrix derivatives, $P_{jb}^{x} = X_{jb}$ and $P_{bj}^{x} = Y_{jb}$. The calculation of the quantities in Eq.10 permits to obtain vibrational frequencies within the harmonic approximation in the QM/FQ/PCM framework, which are required to model VCD spectra. Notice that, in case of nuclear perturbations, the consideration of only the QM moiety of the system in the definition of energy second derivatives in Eq.10 is consistent with the so-called Partial Hessian Vibrational Approach (PHVA),[61–63] which has been amply exploited to treat vibrational phenomena of complex systems.

2.1.1 Mixed electric-magnetic properties

In the presence of an external electric field $\mathbf{E}$ and assuming that the FQs are affected by the field only through the response of the QM molecule, a perturbation term appears in the energy functional

$$V^{ele} = -\boldsymbol{\mu} \cdot \mathbf{E} = -(\boldsymbol{\mu}^n - \sum_{\mu\nu} P_{\mu\nu}\mathbf{M}_{\mu\nu}) \cdot \mathbf{E}$$

where $\mathbf{M}_{\mu\nu} = \langle\chi_\mu|\mathbf{r}|\chi_\nu\rangle$ are dipole integrals (χ_μ and χ_ν denote in this case basis functions). Energy second derivatives with respect to the electric field, therefore reduce to

$$\mathcal{E}^{xy} = \alpha_{xy} = \sum_{\mu\nu} M^x_{\mu\nu} P^y_{\mu\nu} \tag{13}$$

The right-hand side of the CPHF equations becomes:

$$\tilde{Q}^{ele}_{ia} = \tilde{F}^{(x)}_{ia} = \mathbf{M}_{ia} \tag{14}$$

Since the above expression is real, it is possible to reduce the response equations to a problem of half dimension and solve for $\mathbf{X} + \mathbf{Y}$ together

$$(\tilde{\mathbf{A}} + \tilde{\mathbf{B}})(\mathbf{X} + \mathbf{Y}) + 2\mathbf{Q} = 0 \tag{15}$$

which can be used together with $(\tilde{\mathbf{A}} + \tilde{\mathbf{B}})(\mathbf{X} - \mathbf{Y}) = 0$.

In the presence of a static magnetic field, assumed to be given by the sum of a homogenous magnetic field $\mathbf{B}$ and of a field produced by the magnetic moment $\mathbf{m}_X$ of the nucleus X at position $\mathbf{R}_X$, four perturbation terms appear in the Fock operator (the Coulomb Gauge is assumed and minimum coupling is exploited to introduce the magnetic field)

$$h^{(10)}_{\mu\nu} = -\frac{i}{2c}\langle\chi_\mu|(\mathbf{r} \wedge \nabla) \cdot \mathbf{B}|\chi_\nu\rangle \tag{16}$$

$$h_{\mu\nu}^{(01)} = -\frac{i}{c}\langle\chi_\mu|\frac{\mathbf{m}_X \cdot (\mathbf{r} - \mathbf{R}_X)}{|\mathbf{r} - \mathbf{R}_X|^3}|\chi_\nu\rangle \tag{17}$$

$$h_{\mu\nu}^{(11)} = \frac{1}{2c^2}\langle\chi_\mu|\frac{(\mathbf{B} \wedge \mathbf{r}) \cdot [\mathbf{m}_X \wedge (\mathbf{r} - \mathbf{R}_X)]}{|\mathbf{r} - \mathbf{R}_X|^3}|\chi_\nu\rangle \tag{18}$$

$$h_{\mu\nu}^{(20)} = \frac{1}{8c^2}\langle\chi_\mu|(\mathbf{B} \wedge \mathbf{r}) \cdot (\mathbf{B} \wedge \mathbf{r})|\chi_\nu\rangle \tag{19}$$

When working in the London Orbitals' formalism, the basis functions depend on the perturbing field. For this reason no term in equation 10 can be neglected. In case of a magnetic perturbation, the right-hand side of the CPHF is purely imaginary:

$$Q_{ia}^{mag} = h_{ia}^{(x)} + G_{ia}^{(x)}(\mathbf{P}) - G_{ia}(S_{oo}^x) - \mathbf{F}S_{ia}^x \tag{20}$$

and hence $\mathbf{Q_X} = -\mathbf{Q_Y}$. This time it is possible to solve for $\mathbf{X} - \mathbf{Y}$ together by subtracting the response equations

$$(\mathbf{A} - \mathbf{B})(\mathbf{X} - \mathbf{Y}) + 2\mathbf{Q} = 0 \tag{21}$$

which can be used together with $(\mathbf{A} - \mathbf{B})(\mathbf{X} + \mathbf{Y}) = 0$.

After including the contribution for the QM/FQ/PCM the right-hand side of the CPHF equations becomes:

$$Q_{ia}^{mag} = h_{ia}^{(x)} + G_{ia}^{(x)}(\mathbf{P}) - G_{ia}(S_{oo}^x) - \mathbf{F}S_{ia}^x + \mathbf{q}^\dagger \mathbf{V}_{FQ,ia}^x + \boldsymbol{\sigma}^\dagger \mathbf{V}_{PCM,ia}^x \tag{22}$$

2.2 Vibrational Circular Dichroism

Circular Dichroism intensity is related to the difference in attenuation of left and right circularly polarized light passing through a sample. It may be represented by the differential molar extinction coefficient $\Delta\epsilon$,[64–66] given by

$$\Delta\epsilon = \epsilon_L - \epsilon_R \tag{23}$$

where $\epsilon_{L,R}$ refer to left and right circularly polarized light, respectively. Within the framework of the Time-Dependent Perturbation Theory, at a given frequency ν $\Delta\epsilon$ can be calculated as

$$\Delta\epsilon(\nu) = 4\gamma\nu \sum_{i,f} R(i \rightarrow f) f_{if}(\nu_{if}, \nu) \tag{24}$$

where ν_{if} is the frequency of the $i \rightarrow f$ transition (involving vibrational states of the electronic ground state, in case of VCD), γ is a numerical coefficient, $f_{if}(\nu_{if}, \nu)$ is the shape of the absorption band and $R(i \rightarrow f)$ is the rotational strength (RS). Within the harmonic approximation, the latter can be written as

$$R(0 \rightarrow 1)_i = \mathrm{Im}[\langle 0|\mu_{el}|1\rangle_i \langle 0|\mathrm{m}_{mag}|1\rangle_i] \tag{25}$$

The RS is therefore the product of the electric dipole and magnetic dipole transition moments $\langle 0|\mu_{el}|1\rangle_i$ and $\langle 0|\mathrm{m}_{mag}|1\rangle_i$, that can be expressed as

$$\langle 0|(\mu_{el})_\beta|1\rangle_i = \left(\frac{\hbar}{4\pi\nu_i}\right)^{\frac{1}{2}} \sum_{\lambda,\alpha} S_{\lambda\alpha,i} (\mathrm{APT})^\lambda_{\alpha\beta} \tag{26}$$

$$\langle 0|(\mathrm{m}_{mag})_\beta|1\rangle_i = (4\pi\hbar^3\nu_i)^{\frac{1}{2}} \sum_{\lambda,\alpha} S_{\lambda\alpha,i} (\mathrm{AAT})^\lambda_{\alpha\beta} \tag{27}$$

where, according to Stephens,[67] $\mathrm{APT}^\lambda_{\alpha\beta}$ and $\mathrm{AAT}^\lambda_{\alpha\beta}$ are the atomic polar tensor (APT) and atomic axial tensor (AAT), respectively, and $S_{\lambda\alpha,i}$ is a matrix converting Cartesian coordinates X of the nucleus λ into normal coordinates Q

$$Q_i = \sum_{\lambda,\alpha} S_{\lambda\alpha,i} X_{\lambda\alpha} \tag{28}$$

The APT is defined as[67–72]

$$(\mathrm{APT})^{\lambda}_{\alpha\beta} = \qquad E^{\lambda}_{\alpha\beta} + N^{\lambda}_{\alpha\beta} = \\ = 2\left\langle \left(\frac{\partial \Psi_G}{\partial X_{\lambda\alpha}}\right)_{R_0} \middle| (\mu^{e}_{el})_{\beta} \middle| \Psi^{0}_{G} \right\rangle + Z_{\lambda} e \delta_{\alpha\beta} \tag{29}$$

and AAT as

$$(\mathrm{AAT})^{\lambda}_{\alpha\beta} = I^{\lambda}_{\alpha\beta} + J^{\lambda}_{\alpha\beta} = \\ = \left\langle \left(\frac{\partial \Psi_G}{\partial X_{\lambda\alpha}}\right)_{R^0} \middle| \left(\frac{\partial \Psi_G}{\partial B_{\beta}}\right)_{B_{\beta}=0} \right\rangle + \frac{i}{4hc} \sum \varepsilon_{\alpha\beta\gamma} R^{0}_{\lambda\gamma} (Z_{\lambda} e) \tag{30}$$

where μ^{e}_{el} is the electronic part of μ_{el} while $Z_{\lambda}e$ and R^{0}_{λ} are the charge and position of nucleus λ at the equilibrium geometry R^0. Ψ_G is the wave function of the ground electronic state while $(\partial\Psi_G/\partial X_{\lambda\alpha})$ and $(\partial\Psi_G/\partial B_{\beta})$ are the derivatives of the wave function with respect to nuclear displacement and magnetic field, respectively. The former enters into a vibrational transition moment; the latter is appropriate to a magnetic dipole transition moment.

FQ contributions affect the wavefunction and its derivatives. In particular, by solving the CPHF/CPKS equations taking into account FQ/PCM contributions (see Eqs.12 and 21) the APT and AAT in the QM/FQ/PCM framework are obtained.

3 Computational details

The geometry of (R)-methyloxirane ((R)-moxy) was optimized at the B3LYP/ aug-cc-pVDZ level and the C-PCM[73] to represent the aqueous environment (ε = 78.3553). Following what has already been reported by some of the present authors,[17] in order to obtain a representative conformational sampling of solvated (R)-moxy, a 25 ns MD simulation was performed in a pre-equilibrated box of 2175 SPC (Single Point Charge) water molecules in the NPT (isothermal-isobaric) ensemble using GROMACS.[74,76–78] All bonds were kept rigid

using the Settle algorithm[79] for water; the geometry of the solute was kept rigid during the simulation. Electrostatic interactions were considered through the the Particle Mesh Ewald summation method.[80] The pressure was stabilized at 1 bar using the weak-coupling scheme with a coupling constant of 10 ps and an isotherm compressibility of $5 \cdot 10^{-5}\text{bar}^{-1}$. Each component of the system (both methyloxyrane and water) was coupled separately to a temperature bath at 300 K using the Berendsen thermostat[81] with a coupling constant of 0.5 ps. The all-atoms OPLS-AA (Optimized Potentials for Liquid Simulations - All Atoms) force field[82] was used for the solute.

2000 snapshots were extracted from the last 20 ns of the MD simulation (one snapshot every 10 ps). For each snapshot a sphere centered at the solute's geometric center was cut. A cutting radius of 12 Å was used, surrounded by a 1.5 Å larger radius for the PCM spherical cavity. The analysis of the extracted snapshots confirms that they are uncorrelated and constitute a statistically adequate sampling.

The 10 ns MD simulation for (L)-alanine was performed using a similar computational protocol. The box (1 nm edge) contained a single alanine molecule, which was solvated with water molecules modeled using the TIP3P parameter set.[75] The dispersion and repulsion terms were modeled according to the OPLS-AA force field.[82] Electrostatic interactions were taken into account by means of the Particle Mesh Ewald method. The bond vibrations were removed with LINCS algorithm. The pressure was stabilized at 1 bar using the weak-coupling scheme with a coupling constant of 1 ps. Each component of the system (both alanine and water) was coupled separately to a temperature bath at 300 K using the Berendsen thermostat. 1000 snapshots were extracted from the last 5 ns of the MD simulation (one snapshot every 5 ps). For each snapshot a sphere centered at the solute's geometric center was cut (cutting radius of 12 Å). The analysis of the extracted snapshots confirms that they are uncorrelated and constitute a statistically adequate sampling.

The partial optimization of each snapshot for both (R)-methyloxirane and (L)-alanine was performed using the Berny algorithm[83] implemented in the Gaussian package,[84] with water

molecules kept fixed. The calculation of the RMSD related to the structures before and after optimization gives average values of 0.03 Å and 0.40 Å for (R)-methyloxirane and (L)-alanine, respectively, thus showing that the geometry optimization only causes slight changes in the starting molecular geometry. Finally, the VCD spectra were calculated on each partially optimized snapshot with the QM/FQ/PCM model using the B3LYP functional in combination with the aug-cc-pVDZ (R-moxy) and 6-311++G** (L-alanine) basis sets for the solute, the SPC FQ parameters for water[38] and the C-PCM to account for the outer solvent shell. The data were averaged to obtain the final spectra, of which the peaks were convoluted with a Lorentzian lineshape, with Full Width at Half Maximum (FWHM) of 4 cm^{-1}.

The PCM calculations were performed by using the IEF-PCM formalism[21,85,86] with and without the inclusion of cavity field and non-equilibrium effects[87–89] by using the dielectric constants for the aqueous environment $\varepsilon = 78.3553$, $\varepsilon_\infty = 1.777849$.

All QM/FQ/PCM and PCM calculations were performed by using a development version of the Gaussian package,[84] where the QM/FQ/PCM approach here described was implemented.

4 Applications

In this section, the results obtained by applying the QM/FQ/PCM method to two test cases are reported. In particular, the VCD spectra of aqueous solutions of (R)-methyloxirane and (L)-alanine are considered (see Supporting Information for a scheme of their structure). The first system is a classic test of any computational model for chiroptical properties/spectroscopies, for which many previous calculations and experiments are reported in the literature.[90–96] The second system, a simple amino acid, is a minimal prototype of bio-systems, of which the natural environment is the aqueous solution. At the first instance, the calculated QM/FQ/PCM spectra will be compared with calculated results obtained by resorting to continuum solvation models exploiting the PCM approach. The reason for such

a comparison is twofold: in fact, (i) the PCM is currently the most used approach to take into account solvent effects in VCD calculations and (ii) the PCM lacks explicit consideration of specific solute-solvent effects, such as hydrogen bonding. Therefore, the comparison between PCM and QM/FQ/PCM values, obtained by exploiting the same combination of DFT functional and basis set, highlights the role of hydrogen bonding interactions in the simulation of VCD spectra. Also, solvent-induced band broadening is not considered in PCM calculations, for which the reported bands will be artificially broadened by exploiting a Lorentzian function. On the contrary, the QM/FQ/PCM approach, coupled to MD simulations is able to take into account the band broadening which arises from the dynamical description of the solvation phenomenon. In this way also the inhomogenous (due to the fluctuations of the solvent molecules) band broadening contributes to the final shape. Both PCM and QM/FQ/PCM will also be compared with experimentally measured VCD spectra, taken form the recent literature. This latter comparison will immediately give the reader an estimate of the increase in the quality of calculated data, which can be obtained by exploiting our explicit modeling.

4.1 (R)-methyloxirane in aqueous solution

As a first test case, in this section the QM/FQ/PCM approach is applied to the VCD spectrum of (R)-methyloxirane in aqueous solution. In Figure 1 the stick spectrum reporting the VCD intensities obtained for the 2000 snapshots extracted from the MD simulation (see section 3 for details) is plotted: notice that such a stick spectrum is simply obtained by plotting the raw data extracted from the calculations. The corresponding stick infrared (IR) spectrum is reported in Figure S2 in the SI. Figure 1 clearly shows that the VCD signals (both wavenumbers and rotational strengths) depend on the snapshot, i.e. basically on the arrangement of the polarizable water molecules around the solute, whereas the deviation in the structure of the solute across the partially-optimized snapshots is minor (see section 3 for details on the computational protocol to extract and optimize the geometry of the snapshots).

In particular, the peak intensities not only vary in absolute value, but in sign. Also, the sign variability does not affect all the bands to the same extent: in fact the sign of some bands is stable all over the snaphots (time), whereas for some bands a larger variability is apparent. The largest variability is shown by the band between 1450 and 1500 cm^{-1} (see Figures S3-S4 in SI for a pictorial view of the normal modes as calculated with the QM/FQ/PCM for a randomly chosen snapshot or for the minimum PCM structure). The inset in Figure 1 gives a closer look at this region and shows that a comparable number of snapshots have a positive or negative rotational strength, which results in a weak, positive, double band in the average spectrum (see panel b in Figure 2). From the inspection of the stick spectrum it is also clear that the broadening of the spectra bands is already considered in our QM/FQ/PCM approach based on MD snapshots, due to the averaging over the conformational space. Therefore, solvent inhomogeneous broadening (due to the fluctuations of the solvent molecules) does not need to be artificially considered by imposing a pre-defined (and arbitrary) band-width, which is instead necessary when other static approaches are used. We also note that the convergence of the spectrum as a function of the spectrum is amply reached by using 2000 snapshots. Such a number was chosen according to previous studies by some of us[17] on the calculation of the OR of the same system. There, 2000 was reported to be the minimum reasonable number of snapshots to achieve the convergence in the calculated property. In our case, a 10 times smaller number of snapshots (200, chosen in regular time interval, i.e. one every 100 ps) is already adequate to give an averaged spectrum at convergence (see Figure S5 in SI). This might reasonably be related to the more local character of vibrations, i.e. to the stricter link between the property and the solute structure, whereas OR tends to be a global response of the whole system, which also justifies the difficulties in its computational description.[92,93,97–101]

As already commented in previous sections, the currently standard procedure to account for solvation effects on VCD is to resort to the PCM. The PCM spectrum is shown in panel a of Figure 2. Notice that, in order to facilitate the comparison, the reported spectra in

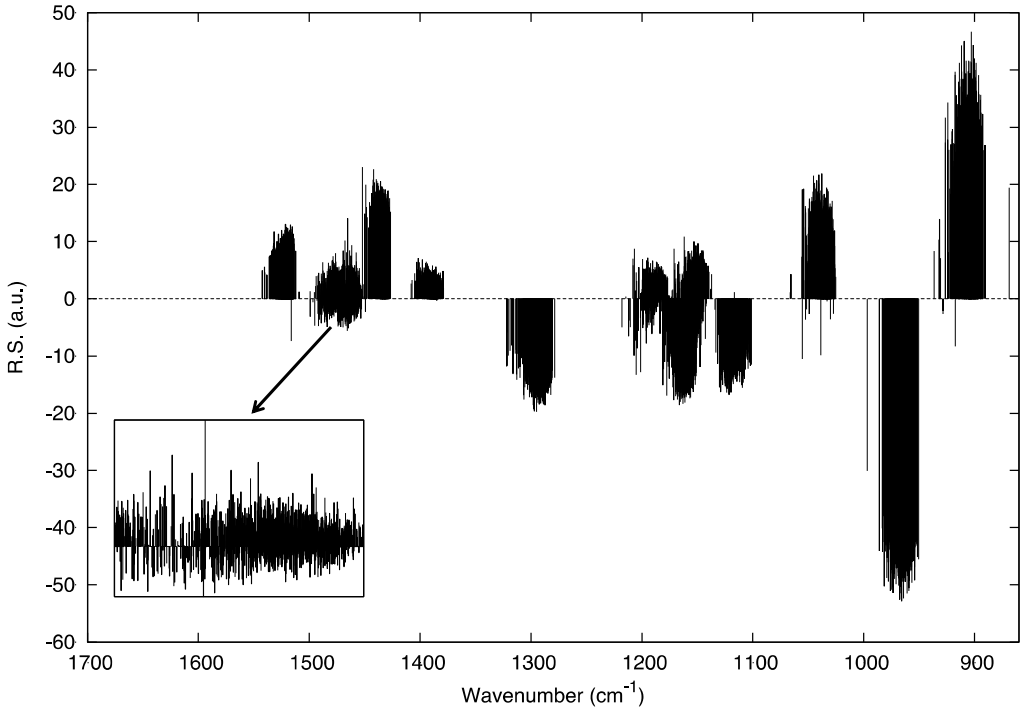

Figure 1: Stick VCD spectrum of (R)-methyloxirane in aqueous solution. An enlarged view of the region between 1450 and 1475 cm^{-1} is given as inset.

Figure 2 have been scaled so that the wavenumbers and intensities of the peak at about 960 cm^{-1} are the same. There are several studies that provide scaling factor to adjust vibrationals frequencies,[102–104] however the majority of the works reported in the literature concern systems in vacuum. As previously reported by one of us[105,106] scaling factors for solvated system may substantially deviate from the corresponding values for isolated systems at a given QM level. In the lack of extensive studies on this matter, our choice for the scaling procedure seems to be the most effective. A three panel showing the same spectra as presented in Figure 2 is reported in Figure S6 of the SI. Raw (non scaled) data are given in Figure S7 of the SI.

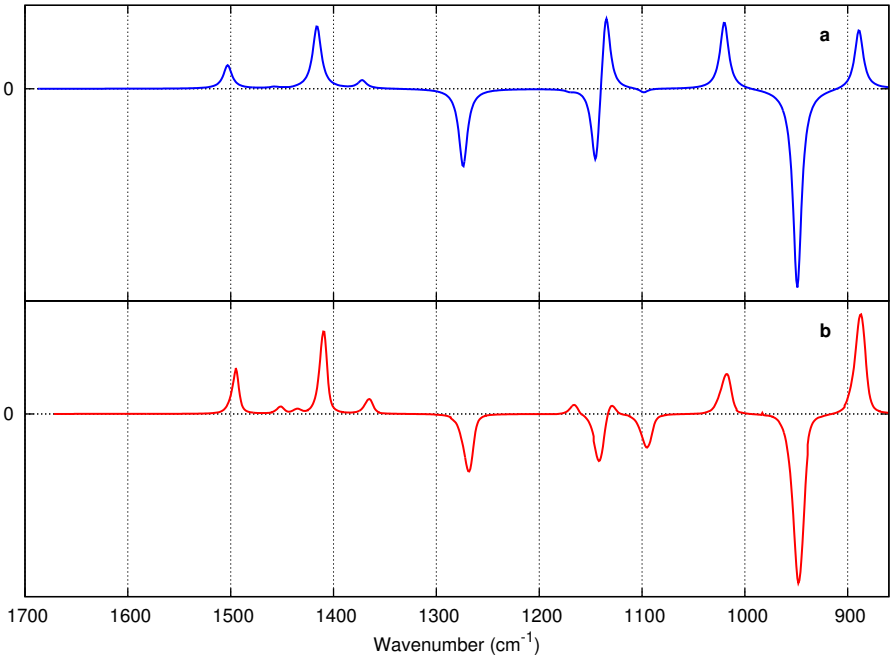

Figure 2: a) PCM and b) QM/FQ/PCM VCD spectra of (R)-methyloxirane in aqueous solution. The reported spectra were scaled so that the peaks at about 960 cm^{-1} have the same wavenumbers and intensities.

The comparison of the spectra in Figure 2 shows that there is a small deviation in peak's (scaled) wavenumbers, however larger deviations are reported for relative intensities, which are differently predicted by the two approaches. The largest differences are noticed for the region between 1050 and 1200 cm^{-1}. In fact, a sharp +/- structure is predicted by the PCM, whereas a more complicated, and by far less intense pattern arises form the application

of the QM/FQ/PCM approach. In order to get more insight into solvent effects, we have performed additional calculations on the structures optimized at the QM/FQ/PCM level, by substituting the explicit external environment with the continuum PCM in the calculation of the VCD Rotational Strengths on the various snapshots. The results of this hybrid approach (see Figure S9 in the SI) show that the leading effects come from specific solvent-induced changes on molecular geometries, rather than on direct solvent effects on the property.

The comparison between the PCM and QM/FQ/PCM approaches with experimental[4] VCD spectra is also presented in Figure 3. The better performance of the QM/FQ/PCM model at reproducing the experimental spectrum is evident, especially as far as the region between 1100 and 1200 cm^{-1} is concerned. In fact, PCM predicts a very small negative peak at about 1110 cm^{-1} and a high positive one at about 1140 cm^{-1}. On the contrary, the QM/FQ/PCM model correctly reproduces this spectral region. Overall, all the intensities and the peaks sign alternation are remarkably well reproduced, thus showing the relevance of exploiting the explicit solvent modeling. The only regions which are badly reproduced (by both methods) regards the peaks at 980, 1070, 1185, 1210, 1460 cm^{-1} and the large positive band between 1600 and 1700 cm^{-1}, which have different signs in the calculated and experimental spectra or are not reproduced at all. This is not surprising, because such peaks have been attributed to the so-called "chirality-transfer" effects to water molecules.[4,107,108] In fact, such signals are due to water normal modes, which gain rotational strength as a result of the strong interaction with methyloxirane. Such modes cannot be accounted for in our QM/FQ/PCM model, which only considers the vibrations of the QM portion of the system. Such modes could have been in principle considered by including selected water molecules in the QM moiety, however the choice of the number and positions of such water molecules is far from being trivial. Efforts towards such an extension are in progress in our lab, and will be the topic of further publications.

Still on the VCD of methyloxirane in aqueous solution, it is worth pointing out that substantial disagreement between PCM and experimental VCD data still remains when a refined

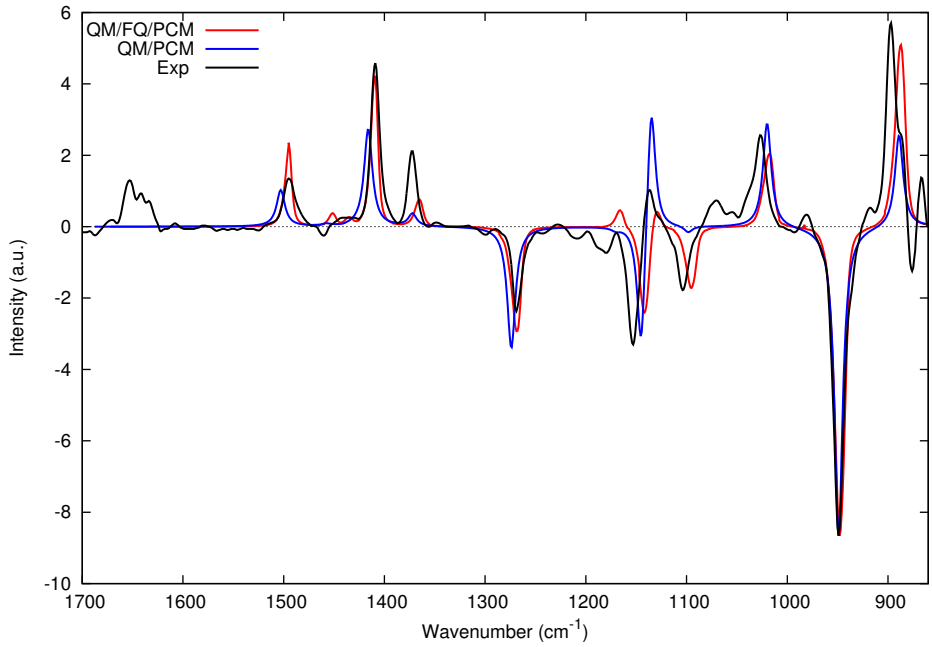

Figure 3: PCM, QM/FQ/PCM and experimental[4] VCD spectra of (R)-methyloxirane in aqueous solution. The calculated spectra were scaled so that the peaks at about 960 cm^{-1} have the same wavenumbers and intensities.

version of the PCM[109] for the description of VCD spectra[87] is exploited, also considering vibrational nonequilibrium[88] and cavity field[110] effects (see Figure S8 given as Supporting information).

To end the discussion on the VCD of methyloxirane in aqueous solution, in order to evaluate the relevance of polarization effects in our QM/FQ/PCM approach, a comparison with a non polarizable QM/MM/PCM (exploiting TIP3P[75] charges for water molecules) has been performed. The results for 200 snapshots are shown in Figure 4. It is clearly shown that the two calculated spectra are in this case very similar. However the quality of such a comparison is expected to strongly depend upon the nature of the system, i.e. polarization may affect different molecular systems to a different extent (vide infra).

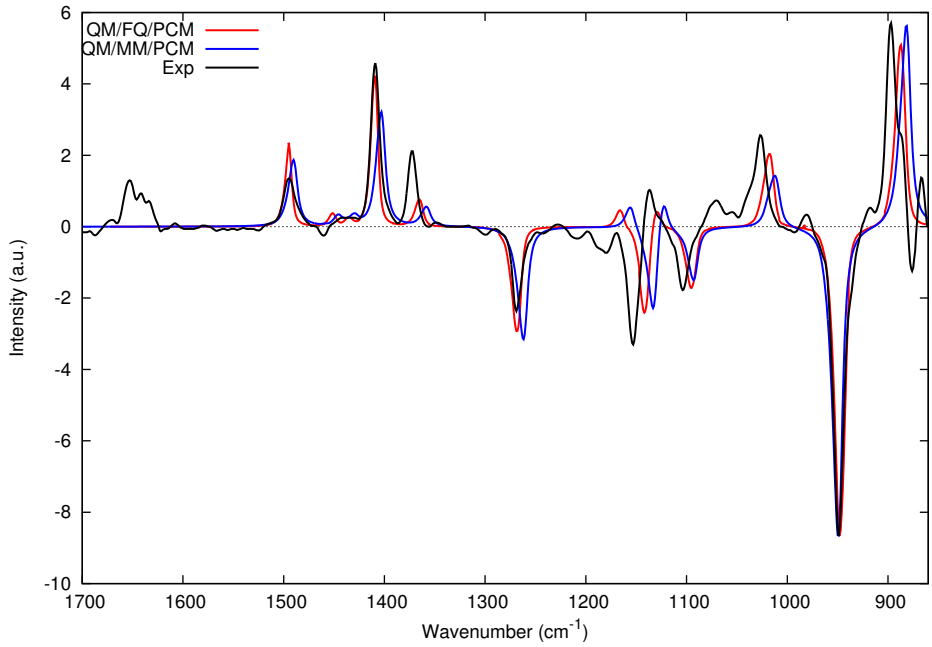

Figure 4: Non polarizable QM/MM/PCM (TIP3P[75] charges), QM/FQ/PCM and experimental[4] VCD spectra of (R)-methyloxirane in aqueous solution. The calculated spectra were scaled so that the peaks at about 960 cm^{-1} have the same wavenumbers and intensities.

4.2 (L)-Alanine in aqueous solution

The second studied system is (L)-alanine (L-ALA) in aqueous solution (see Figure S10 in SI). This is the smallest chiral aminoacid and as the others occurs in the zwitterionic form in aqueous solution, that is its natural environment. The VCD spectrum of L-ALA in aqueous solution has been studied both from a theoretical and an experimental point of view, and it was the first system for which vibrational optical activity techniques were applied.[111–122] However, to the best of our knowledge, this is the first time that the VCD spectrum of this molecule is studied by the combination of classical MD and a QM/MM approaches.

The most interesting range in the VCD spectrum for this molecule has been shown to be that between 1250 and 1450 cm^{-1}, since the VCD signal is mostly zero in the other regions. As pointed out by Nafie,[10] this region is characterized by a (+,-,+) triplet of modes near 1410, 1360, 1300 cm^{-1}, representing the symmetric stretching of the CO_2^- group and a pair of orthogonal methine CH bending modes.

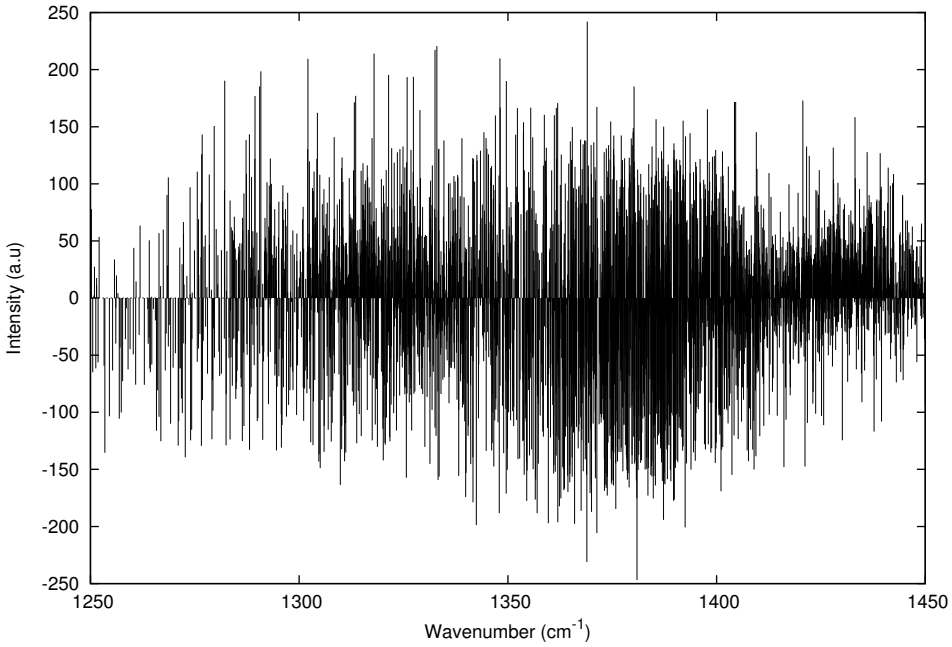

Figure 5: QM/FQ/PCM stick spectrum of (L)-alanine in aqueous solution at the B3LYP/6-311++G** level of theory. The QM/FQ/PCM calculations was performed on 1000 snapshots extracted from the MD.

Figure 5 reports calculated rotational strengths as a function of the snapshots extracted from the MD (IR spectra are given in Figure S11 in Supporting Information). A large variability, in both sign and in magnitude, is evident, and the range of variation spans a by far greater interval (one order of magnitude larger) with respect to what was shown in the previous section for methyloxirane. This immediately predicts a greater difficulty in modeling this spectrum by using static approaches, such as the PCM. In fact, as it is clearly shown by the data in Figure 6, the PCM and averaged QM/FQ/PCM spectra are completely different (see also Figure S13 for the same spectra in a three panel figure and Figure S14 in SI for non-scaled spectra). It is especially interesting to notice a complete disagreement in the predicted sign of the peak at about 1310 cm^{-1} and an extremely larger positive band predicted by PCM in the region between 1370 and 1400 cm^{-1}. Figure 6 also shows the experimental VCD spectrum measured by Diem:[120] the good agreement between the experimental and our QM/FQ/PCM spectra is evident. This can be even better appreciated in Figure 7, where the off-peaks given by PCM, and which flatten other spectra, are not shown. The only troublesome aspect for

our model is an inaccurate prediction of the relative intensities of the two positive peaks at 1300 cm^{-1} and 1410 cm^{-1}, for which the sign is nevertheless correctly reproduced. To end this discussion it is worth remarking that, similarly to what was already commented for methyloxirane, the inclusion of vibrational nonequilibrium[88] and cavity field[110] effects on the calculation of PCM-VCD spectra does not substantially improve the description of the experimental spectrum (see Figure S14 in Supporting Information). Moreover, the completely different behavior between PCM and QM/FQ/PCM results (Figure 6) can also be attributed to the relevance of explicit solvent effects on the molecular geometry, as it is demonstrated by the RMSD value of 0.4 Å , which is still small but significantly larger than what we have observed for methyloxirane.

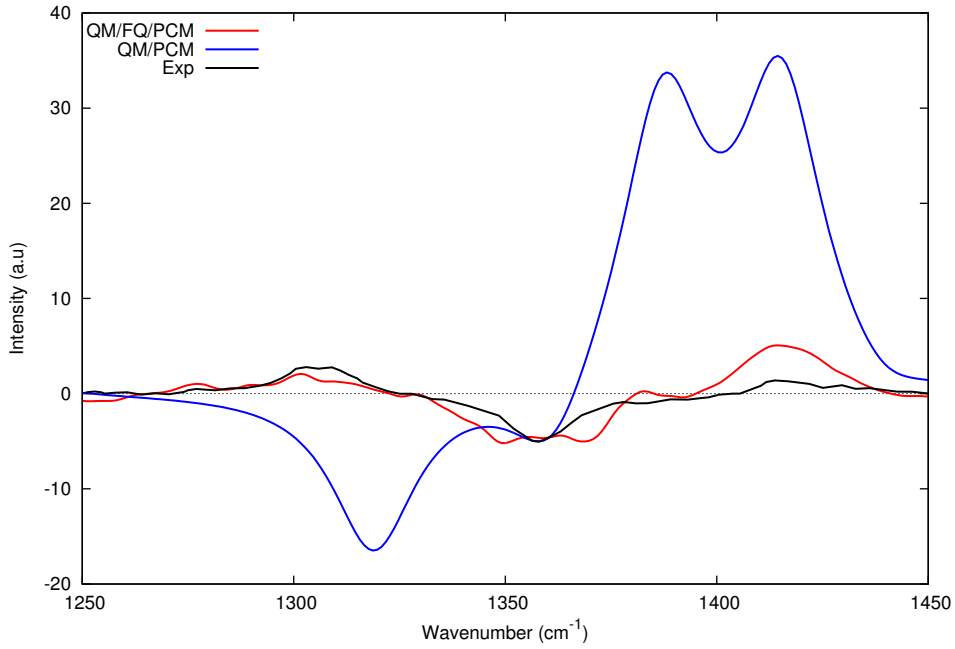

Figure 6: Comparison between the experimental[120](black), QM/FQ/PCM (red), PCM (blue) spectra of (L)-alanine in aqueous solution. The calculations were performed at the B3LYP/6-311++G** level of theory. The PCM spectrum is drawn by considering a FWHM of 12 cm^{-1}. QM/FQ/PCM and PCM spectra are scaled so that the negative peaks at about 1360 cm^{-1} have the same wavenumbers and intensities. The corresponding non-scaled spectra are reported in Figure S10 given as Supporting Information.

To conclude the discussion on (L)-alanine in aqueous solution, as before for (R)-methyloxirane, a comparison between a non polarizable QM/MM/PCM (TIP3P charges) and our model has

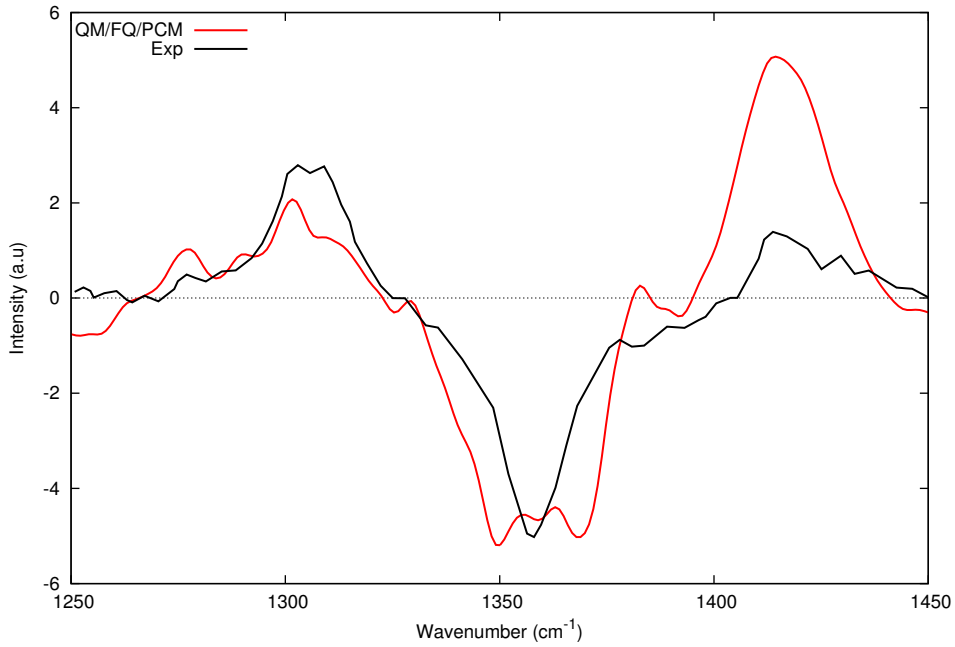

Figure 7: Comparison between the experimental[120](black) and QM/FQ/PCM (red) spectra of (L)-alanine in aqueous solution. The calculations were performed at the B3LYP/6-311++G** level of theory. QM/FQ/PCM spectrum is scaled so that the negative peak at about 1360 cm^{-1} has the same wavenumber and intensity as in the experiment.

been performed. The results are shown in Figure 8. Differently from methyloxirane, in the present case the inclusion of polarization largely affects the final spectra. In fact, the high positive pick at about 1340 cm^{-1} and the two negative ones at about 1270 and 1420 cm^{-1} predicted by the non-polarizable approach have no correspondences in the experimental spectrum, which presents only a (+,-,+) alternation. Such a different behaviour observed for the two test systems here investigated may be probably due to the zwitterionic character of (L)-alanine, for which the two (polarizable and non-polarizable) approaches yield a different description.

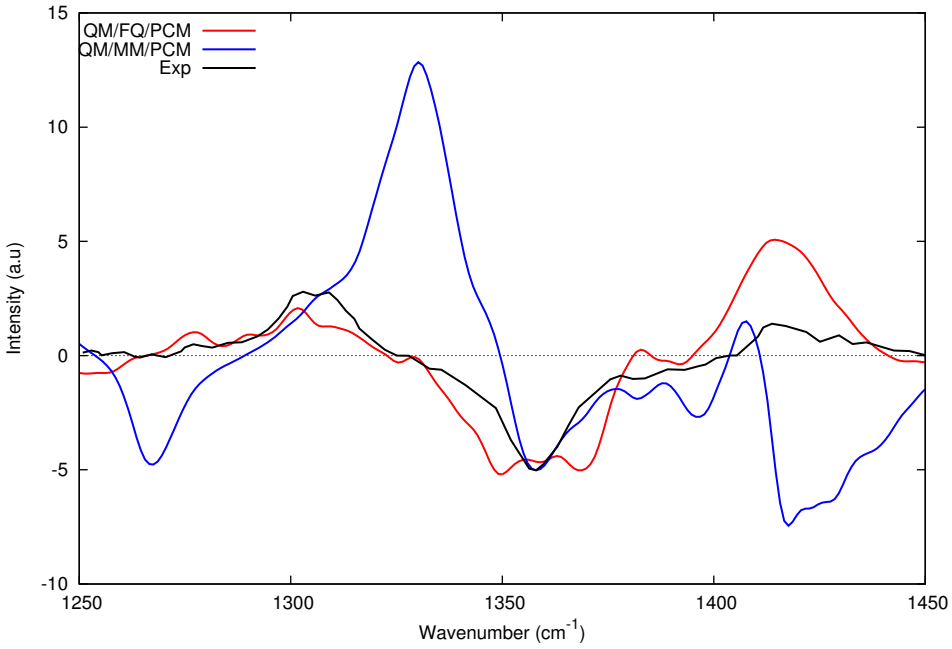

Figure 8: Comparison between the experimental[120](black), QM/FQ/PCM (red) and QM/MM/PCM (blue) spectra of (L)-alanine in aqueous solution. The calculations were performed at the B3LYP/6-311++G** level of theory. QM/FQ/PCM and QM/MM/PCM spectra are scaled so that the negative peak at about 1360 cm^{-1} has the same wavenumber and intensity as in the experiment.

5 Summary, Conclusions and Future Perspectives

In this paper, a multi-scale methodology based on the combination of classical MD simulations with a fully polarizable QM/FQ/PCM Hamiltonian is extended to the calculation of VCD spectra of chiral systems in aqueous solution. This mixed explicit/implicit approach is able to account for solute-solvent mutual polarization effects and the dynamical aspects of the solute-solvent interaction. Also, the QM/FQ/PCM calculation of the VCD spectrum ensures an accurate description of the electronic density of the solute and a proper account for the specific solute-solvent interactions. The computational cost of our approach is, as far as the single calculation of a snapshot is concerned, the same as that required for the corresponding PCM calculation. Obviously, the final computational cost strongly depends on the number of snapshots which have to be considered to reach the convergence of the desired property. The application of the proposed approach to the VCD spectra of (R)-methyloxirane and (L)-alanine in aqueous solution shows remarkable agreement between calculated and experimental spectra, and notably a substantial improvement with respect to the description of the solute-solvent interaction given by the continuum PCM approach. Some feature of the experimental spectra, due to the so-called "chirality-transfer" effects to solvent molecules, cannot be reproduced, due to the fact that such signals are connected to the vibrational modes of solvent molecules, which gain rotational strength as a result of the strong interaction with the target system. Such modes cannot be accounted for in the basic QM/FQ/PCM model here presented, which only considers the vibrations of the QM portion of the system. Such modes could have been in principle considered by including selected solvent molecules in the QM moiety, however the number and positions of such solvent molecules are hardly predictable.

Although the results reported in the present paper are promising, an extensive and general application of this methodology will require extension to non-aqueous environments, for which effects due to the so-called chiral imprint [123] have been often invoked. Such an extension will require not only an adequate parametrization of the FQ force field for the various

solvating environments, but also the consideration of non-electrostatic interactions. Some steps towards this direction have been done for other families of multi-scale methods,[124–127] and a similar extension of the QM/FQ/PCM approach will be necessary to enlarge the spectrum of possible applications.

Acknowledgements

MO and CC acknowledge support from the Italian MIUR (PRIN 2012 NB3KLK002) and COST CMST-Action CM1405 MOLecules In Motion (MOLIM). The HPC computational facilities available at the SMART@SNS Lab are also acknowledged.

Supporting Information

Molecular structures of (R)-Methyloxirane and (L)-Alanine. PCM and QM/FQ/PCM IR spectra and normal modes of both molecules. (R)-Methyloxirane VCD spectrum calculated by using 2000 snapshots and 200 snapshots. Non-scaled VCD data for both molecules. PCM VCD spectra calculated by adding cavity field and non-equilibrium contributions. (R)-Methyloxirane QM/PCM VCD spectrum obtained by applying the PCM to selected optimized QM/FQ/PCM structures. This information is available free of charge via the Internet at http://pubs.acs.org.

References

(1) Berova, N., Polavarapu, P. L., Nakanishi, K., Woody, R. W., Eds. *Comprehensive Chiroptical Spectroscopy*; Wiley, New York, 2012.

(2) Losada, M.; Xu, Y. *Phys. Chem. Chem. Phys.* **2007**, *9*, 3127–3135.

(3) Losada, M.; Tran, H.; Xu, Y. *J. Chem. Phys.* **2008**, *128*, 014508.

(4) Losada, M.; Nguyen, P.; Xu, Y. *J. Phys. Chem A* **2008**, *112*, 5621–5627.

(5) Yang, G.; Xu, Y. *J. Chem. Phys.* **2009**, *130*, 164506–164506.

(6) Poopari, M. R.; Zhu, P.; Dezhahang, Z.; Xu, Y. *J. Chem. Phys.* **2012**, *137*, 194308.

(7) Longhi, G.; Castiglioni, E.; Abbate, S.; Lebon, F.; Lightner, D. A. *Chirality* **2013**, *25*, 589–599.

(8) Berova, N.; Di Bari, L.; Pescitelli, G. *Chem. Soc. Rev.* **2007**, *36*, 914–931.

(9) Polavarapu, P. *J. Phys. Chem.* **1990**, *94*, 8106–8112.

(10) Nafie, L. A. *Vibrational optical activity: principles and applications*; John Wiley & Sons: Chichester, 2011.

(11) Jose, K. J.; Beckett, D.; Raghavachari, K. *J. Chem. Theory Comput.* **2015**, *11*, 4238–4247.

(12) Jose, K. J.; Raghavachari, K. *J. Chem. Theory Comput.* **2016**, *12*, 585–594.

(13) Polavarapu, P. L. *Chem. Rec.* **2007**, *7*, 125–136.

(14) Autschbach, J. *Chirality* **2009**, *21*, E116–E152.

(15) Stephens, P.; Devlin, F.; Chabalowski, C.; Frisch, M. J. *J. Phys. Chem.*. **1994**, *98*, 11623–11627.

(16) Egidi, F.; Barone, V.; Bloino, J.; Cappelli, C. *J. Chem. Theory Comput.* **2012**, *8*, 585–597.

(17) Lipparini, F.; Egidi, F.; Cappelli, C.; Barone, V. *J. Chem. Theory Comput.* **2013**, *9*, 1880–1884.

(18) Bloino, J.; Barone, V. *J. Chem. Phys.* **2012**, *136*, 124108.

(19) Cappelli, C.; Bloino, J.; Lipparini, F.; Barone, V. *J. Phys. Chem.. Lett.* **2012**, *3*, 1766–1773.

(20) Merten, C.; Bloino, J.; Barone, V.; Xu, Y. *J. Phys. Chem.. Lett.* **2013**, *4*, 3424–3428.

(21) Tomasi, J.; Mennucci, B.; Cammi, R. *Chem. Rev.* **2005**, *105*, 2999–3093.

(22) Egidi, F.; Giovannini, T.; Piccardo, M.; Bloino, J.; Cappelli, C.; Barone, V. *J. Chem. Theory Comput.* **2014**, *10*, 2456–2464.

(23) Warshel, A.; Levitt, M. *J. Mol. Biol.* **1976**, *103*, 227–249.

(24) Gao, J.; Xia, X. *Science* **1992**, *258*, 631–635.

(25) Lin, H.; Truhlar, D. *Theor. Chem. Acc.* **2007**, *117*, 185–199.

(26) Cappelli, C.; Mennucci, B. *J. Phys. Chem. B* **2008**, *112*, 3441–3450.

(27) Cappelli, C.; Mennucci, B.; Monti, S. *J. Phys. Chem. A* **2005**, *109*, 1933–1943.

(28) Egidi, F.; Bloino, J.; Cappelli, C.; Barone, V. *Chirality* **2013**, *25*, 701–708.

(29) Cappelli, C. *Int. J. Quantum Chem.* **2016**, DOI: 10.1002/qua.25199.

(30) Sánchez, M. L.; Aguilar, M. A. ; Olivares del Valle, F. J. *J. Comput. Chem.* **1997**, *18*, 313–322.

(31) Monari, A.; Rivail, J. L.; Assfeld, X. *Acc. Chem. Res.* **2013**, *46*, 596–603.

(32) Sjöqvist, J.; Linares, M.; Mikkelsen, K. V.; Norman, P. *J. Phys. Chem. A* **2014**, *118*, 3419–3428.

(33) Gattuso, H.; Assfeld, X.; Monari, A. *Theo. Chem. Acc.* **2015**, *134*, 1–8.

(34) Parac, M.; Doerr, M.; Marian, C. M.; Thiel, W. *J. Comput. Chem.* **2010**, *31*, 90–106.

(35) Jurinovich, S.; Curutchet, C.; Mennucci, B. *ChemPhysChem* **2014**, *15*, 3194–3204.

(36) Patwardhan, S.; Tonzani, S.; Lewis, F. D.; Siebbeles, L. D. A.; Schatz, G. C.; Grozema, F. C. *J. Phys. Chem. B* **2012**, *116*, 11447–11458.

(37) Halgren, T. A.; Damm, W. *Curr. Opinion Struct. Biol.* **2001**, *11*, 236–242.

(38) Rick, S. W.; Stuart, S. J.; Berne, B. J. *J. Chem. Phys.* **1994**, *101*, 6141–6156.

(39) Rick, S. W.; Stuart, S. J.; Bader, J. S.; Berne, B. *J. Mol. Liq.* **1995**, *65*, 31–40.

(40) Rick, S. W.; Berne, B. J. *J. Am. Chem. Soc.* **1996**, *118*, 672–679.

(41) Sanderson, R. *Science* **1951**, *114*, 670–672.

(42) Lipparini, F.; Barone, V. *J. Chem. Theory Comp.* **2011**, *7*, 3711–3724.

(43) Lipparini, F.; Cappelli, C.; Barone, V. *J. Chem. Theory Comput.* **2012**, *8*, 4153–4165.

(44) Lipparini, F.; Cappelli, C.; Scalmani, G.; De Mitri, N.; Barone, V. *J. Chem. Theory Comput.* **2012**, *8*, 4270–4278.

(45) Lipparini, F.; Cappelli, C.; Barone, V. *J. Chem. Phys.* **2013**, *138*, 234108.

(46) Kongsted, J.; Pedersen, T. B.; Strange, M.; Osted, A.; Hansen, A. E.; Mikkelsen, K. V.; Pawlowski, F.; Jørgensen, P.; Hättig, C. *Chem. Phys. Lett.* **2005**, *401*, 385–392.

(47) Kongsted, J.; Ruud, K. *Chem. Phys. Lett.* **2008**, *451*, 226–232.

(48) Egidi, F.; Russo, R.; Carnimeo, I.; D'Urso, A.; Mancini, G.; Cappelli, C. *J. Phys. Chem. A* **2015**, *119*, 5396–5404.

(49) Egidi, F.; Carnimeo, I.; Cappelli, C. *Opt. Mat. Expr.* **2015**, *5*, 196–209.

(50) Cheeseman, J. R.; Shaik, M. S.; Popelier, P. L.; Blanch, E. W. *J. Am. Chem. Soc.* **2011**, *133*, 4991–4997.

(51) Mortier, W. J.; Van Genechten, K.; Gasteiger, J. *J. Am. Chem. Soc.* **1985**, *107*, 829–835.

(52) Chelli, R.; Procacci, P. *J. Chem. Phys.* **2002**, *117*, 9175–9189.

(53) Rappe, A.; Goddard, W. *J. Phys. Chem.* **1991**, *95*, 3358–3363.

(54) York, D. M.; Yang, W. *J. Chem. Phys.* **1996**, *104*, 159–172.

(55) Chelli, R.; Schettino, V.; Procacci, P. *J. Chem. Phys.* **2005**, *122*, 234107.

(56) Ohno, K. *Theor. Chim. Acta* **1964**, *2*, 219–227.

(57) McWeeny, R. *Methods of molecular quantum mechanics*; Academic press: London, 1992.

(58) Barone, V.; Bloino, J.; Guido, C. A.; Lipparini, F. *Chem. Phys. Lett.* **2010**, *496*, 157–161.

(59) Lipparini, F.; Scalmani, G.; Mennucci, B.; Frisch, M. J. *J. Chem. Theory Comput.* **2011**, *7*, 610–617.

(60) Frisch, M.; Head-Gordon, M.; Pople, J. *Chem. Phys.* **1990**, *141*, 189–196.

(61) Jin, S.; Head, J. D. *Surf. Science* **1994**, *318*, 204–216.

(62) Calvin, M. D.; Head, J. D.; Jin, S. *Surf. Science* **1996**, *345*, 161–172.

(63) Biancardi, A.; Cammi, R.; Cappelli, C.; Mennucci, B.; Tomasi, J. *Theor. Chem. Acc.* **2012**, *131*, 1–10.

(64) Stephens, P. J. *J. Phys. Chem.* **1985**, *89*, 748–752.

(65) Stephens, P. J. *J. Phys. Chem.* **1987**, *91*, 1712–1715.

(66) Stephens, P.; Lowe, M. *Ann. Rev. Phys. Chem.* **1985**, *36*, 213–241.

(67) Stephens, P.; Devlin, F. *Chirality* **2000**, *12*, 172–179.

(68) Amos, R.; Handy, N.; Jalkanen, K.; Stephens, P. *Chem. Phys. Lett.* **1987**, *133*, 21–26.

(69) Kawiecki, R.; Devlin, F.; Stephens, P.; Amos, R. *J. Phys. Chem* **1991**, *95*, 9817–9831.

(70) Cheeseman, J.; Frisch, M.; Devlin, F.; Stephens, P. *Chem. Phys. Lett.* **1996**, *252*, 211–220.

(71) Stephens, P. J.; Devlin, F. J.; Pan, J.-J. *Chirality* **2008**, *20*, 643–663.

(72) Stephens, P. J.; Devlin, F. J.; Cheeseman, J. R. *VCD spectroscopy for organic chemists*; CRC Press: Boca Raton, 2012.

(73) Barone, V.; Cossi, M. *J. Phys. Chem A* **1998**, *102*, 1995–2001.

(74) Berendsen, H.; van der Spoel, D.; van Drunen, R. *Comp. Phys. Comm.* **1995**, *91*, 43 – 56.

(75) Berendsen, H.; Postma, J.; van Gunsteren, W.; Hermans, J. in *Intermolecular Forces* **1981**, 331.

(76) Lindahl, E.; Hess, B.; van der Spoel, D. *J. Mol. Model.* **2001**, *7*, 306–317.

(77) Van Der Spoel, D.; Lindahl, E.; Hess, B.; Groenhof, G.; Mark, A. E.; Berendsen, H. J. C. *J. Comput. Chem.* **2005**, *26*, 1701–1718.

(78) Hess, B.; Kutzner, C.; van der Spoel, D.; Lindahl, E. *J. Chem. Theory Comput.* **2008**, *4*, 435–447.

(79) Miyamoto, S.; Kollman, P. A. *J. Comput. Chem* **1992**, *13*, 952–962.

(80) Darden, T.; York, D.; Pedersen, L. *J. Chem. Phys.* **1993**, *98*, 10089 – 10092.

(81) Berendsen, H. J.; Postma, J. P. M.; van Gunsteren, W. F.; DiNola, A.; Haak, J. *J. Chem. Phys.* **1984**, *81*, 3684–3690.

(82) Jorgensen, W. L.; Maxwell, D. S.; Tirado-Rives, J. *J. Am. Chem. Soc.* **1996**, *118*, 11225–11236.

(83) Li, X.; Frisch, M. J. *J. Chem. Theory Comput.* **2006**, *2*, 835–839.

(84) Frisch, M. J.; Trucks, G. W.; Schlegel, H. B.; Scuseria, G. E.; Robb, M. A.; Cheeseman, J. R.; Scalmani, G.; Barone, V.; Mennucci, B.; Petersson, G. A.; Nakatsuji, H.; Caricato, M.; Li, X.; Hratchian, H. P.; Izmaylov, A. F.; Bloino, J.; Janesko, B. G.; Lipparini, F.; Zheng, G.; Sonnenberg, J. L.; Liang, W.; Hada, M.; Ehara, M.; Toyota, K.; Fukuda, R.; Hasegawa, J.; Ishida, M.; Nakajima, T.; Honda, Y.; Kitao, O.; Nakai, H.; Vreven, T.; Montgomery, J., Jr.; Peralta, J. E.; Ogliaro, F.; Bearpark, M.; Heyd, J. J.; Brothers, E.; Kudin, K. N.; Staroverov, V. N.; Keith, T.; Kobayashi, R.; Normand, J.; Raghavachari, K.; Rendell, A.; Burant, J. C.; Iyengar, S. S.; Tomasi, J.; Cossi, M.; Rega, N.; Millam, J. M.; Klene, M.; Knox, J. E.; Cross, J. B.; Bakken, V.; Adamo, C.; Jaramillo, J.; Gomperts, R.; Stratmann, R. E.; Yazyev, O.; Austin, A. J.; Cammi, R.; Pomelli, C.; Ochterski, J. W.; Martin, R. L.; Morokuma, K.; Zakrzewski, V. G.; Voth, G. A.; Salvador, P.; Dannenberg, J. J.; Dapprich, S.; Parandekar, P. V.; Mayhall, N. J.; Daniels, A. D.; Farkas, O.; Foresman, J. B.; Ortiz, J. V.; Cioslowski, J.; ; Fox, D. J. Gaussian 09 Development Version and Revision H.37p. Gaussian Inc. Wallingford CT 2010.

(85) Cances, E.; Mennucci, B.; Tomasi, J. *J. Chem. Phys.* **1997**, *107*, 3032–3041.

(86) Tomasi, J.; Mennucci, B.; Cances, E. *J. Mol. Struct.: THEOCHEM* **1999**, *464*, 211–226.

(87) Cappelli, C.; Corni, S.; Mennucci, B.; Cammi, R.; Tomasi, J. *J. Phys. Chem A* **2002**, *106*, 12331–12339.

(88) Cappelli, C.; Lipparini, F.; Bloino, J.; Barone, V. *J. Chem. Phys.* **2011**, *135*, 104505.

(89) Cappelli, C.; Corni, S.; Cammi, R.; Mennucci, B.; Tomasi, J. *J. Chem. Phys.* **2000**, *113*, 11270–11279.

(90) Barone, V.; Biczysko, M.; Bloino, J.; Puzzarini, C. *J. Chem. Phys.* **2014**, *141*, 034107.

(91) Hodecker, M.; Biczysko, M.; Dreuw, A.; Barone, V. *J. Chem. Theory Comput.* **2016**,

(92) Ruud, K.; Zanasi, R. *Angew. Chem. Int. Ed.* **2005**, *117*, 3660–3662.

(93) Tam, M. C.; Russ, N. J.; Crawford, T. D. *J. Chem. Phys.* **2004**, *121*, 3550–3557.

(94) Mukhopadhyay, P.; Zuber, G.; Goldsmith, M.-R.; Wipf, P.; Beratan, D. N. *Chem. Phys. Chem* **2006**, *7*, 2483–2486.

(95) Carnell, M.; Peyerimhoff, S.; Breest, A.; Gödderz, K.; Ochmann, P.; Hormes, J. *Chem. Phys. Lett.* **1991**, *180*, 477–481.

(96) McGuire, B. A.; Carroll, P. B.; Loomis, R. A.; Finneran, I. A.; Jewell, P. R.; Remijan, A. J.; Blake, G. A. *Science* **2016**, *352*, 1449–1452.

(97) Crawford, T. D.; Tam, M. C.; Abrams, M. L. *J. Phys. Chem. A* **2007**, *111*, 12057–12068.

(98) Pedersen, T. B.; Kongsted, J.; Crawford, T. D.; Ruud, K. *J. Chem. Phys.* **2009**, *130*, 034310.

(99) Caricato, M. *J. Chem. Phys.* **2013**, *139*, 114103.

(100) Wiberg, K. B.; Caricato, M.; Wang, Y.-G.; Vaccaro, P. H. *Chirality* **2013**, *25*, 606–616.

(101) Lahiri, P.; Wiberg, K. B.; Vaccaro, P. H.; Caricato, M.; Crawford, T. D. *Angew. Chem. Int. Ed.* **2014**, *53*, 1386–1389.

(102) Andersson, M. P.; Uvdal, P. *J. Phys. Chem A* **2005**, *109*, 2937–2941.

(103) Merrick, J. P.; Moran, D.; Radom, L. *J. Phys. Chem A* **2007**, *111*, 11683–11700.

(104) Sinha, P.; Boesch, S. E.; Gu, C.; Wheeler, R. A.; Wilson, A. K. *J. Phys. Chem A* **2004**, *108*, 9213–9217.

(105) Cappelli, C.; Silva, C. O.; Tomasi, J. *J. Mol. Struct.: THEOCHEM* **2001**, *544*, 191–203.

(106) Cappelli, C.; Monti, S.; Scalmani, G.; Barone, V. *J. Chem. Theory Comput.* **2010**, *6*, 1660–1669.

(107) Scherrer, A.; Agostini, F.; Sebastiani, D.; Gross, E. K. U.; Vuilleumier, R.*J. Chem. Phys.* **2015**, *143*, 074106.

(108) Scherrer, A.; Vuilleumier, R.; Sebastiani, D. *J. Chem. Phys.* **2016**, *145*, 084101.

(109) Egidi, F.; Cappelli, C. *Elsevier Reference Module in Chemistry, Molecular Sciences and Chemical Engineering* **2015**, DOI: 0.1016/B978–0–12–409547–2.10881–9.

(110) Cammi, R.; Cappelli, C.; Corni, S.; Tomasi, J. *J. Phys. Chem. A* **2000**, *104*, 9874–9879.

(111) Lal, B. B.; Diem, M.; Polavarapu, P. L.; Oboodi, M.; Freedman, T. B.; Nafie, L. A. *J. Am. Chem. Soc.* **1982**, *104*, 3336–3342.

(112) Diem, M.; Polavarapu, P. L.; Oboodi, M.; Nafie, L. A. *J. Am. Chem. Soc.* **1982**, *104*, 3329–3336.

(113) Ellzy, M. W.; Jensen, J. O.; Hameka, H. F.; Kay, J. G. *Spectrochim. Acta A* **2003**, *59*, 2619 – 2633.

(114) Orestes, E.; Bistafa, C.; Rivelino, R.; Canuto, S. *J. Phys. Chem. A* **2015**, *119*, 5099–5106.

(115) Diem, M.; Photos, E.; Khouri, H.; Nafie, L. A. *J. Am. Chem. Soc.* **1979**, *101*, 6829–6837.

(116) Devlin, F.; Stephens, P. *Appl. Spectrosc.* **1987**, *41*, 1142–1144.

(117) Diem, M. Solution conformation of biomolecules from infrared vibrational circular dichroism spectroscopy. Optics, Electro-Optics, and Laser Applications in Science and Engineering. 1991; pp 28–36.

(118) Jalkanen, K.; Degtyarenko, I.; Nieminen, R.; Cao, X.; Nafie, L.; Zhu, F.; Barron, L. *Theo. Chem. Acc.* **2008**, *119*, 191–210.

(119) Frimand, K.; Bohr, H.; Jalkanen, K. J.; Suhai, S. *Chem. Phys.* **2000**, *255*, 165–194.

(120) Diem, M. *J. Am. Chem. Soc.* **1988**, *110*, 6967–6970.

(121) Freedman, T. B.; Diem, M.; Polavarapu, P. L.; Nafie, L. A. *J. Am. Chem. Soc.* **1982**, *104*, 3343–3349.

(122) Diem, M.; Gotkin, P. J.; Kupfer, J. M.; Tindall, A. G.; Nafie, L. A. *J. Am. Chem. Soc.* **1977**, *99*, 8103–8104.

(123) Mukhopadhyay, P.; Zuber, G.; Wipf, P.; Beratan, D. N. *Angew. Chem. Int. Ed.* **2007**, *46*, 6450–6452.

(124) Pruitt, S. R.; Bertoni, C.; Brorsen, K. R.; Gordon, M. S. *Acc. Chem. Res.* **2014**, *47*, 2786–2794.

(125) Pruitt, S. R.; Steinmann, C.; Jensen, J. H.; Gordon, M. S. *J. Chem. Theory Comput.* **2013**, *9*, 2235–2249.

(126) Gordon, M. S.; Fedorov, D. G.; Pruitt, S. R.; Slipchenko, L. V. *Chem. Rev.* **2012**, *112*, 632–672.

(127) Smith, Q. A.; Ruedenberg, K.; Gordon, M. S.; Slipchenko, L. V. *J. Chem. Phys.* **2012**, *136*, 244107

.

For Table of Contents Only